Development of the Data Acquisition and Communications System of a Wave Energy Conversion Buoy for Oceanographic Applications

Leandro Henrique Costa Sousa
leandro.sousa@tecnico.ulisboa.pt

Instituto Superior Técnico, Universidade de Lisboa, Portugal
November 2018

Abstract

This project aims to build a data acquisition system integrated into a wave energy conversion buoy, using low-cost sensors and computer. This dissertation starts by identifying some of the most important parameters to measure and the main concepts and theoretical structure of a data acquisition system. Sensors of temperature, humidity, acceleration angular velocity and magnetic field along with a single-board computer, for the data processing, were used. Given that the acquired signals from the sensors incorporate noise, a Legendre based cascade filter was implemented. This filter was developed for this project. The cascade filter achieved a better attenuation than the elementary filters and a very narrow transition bandwidth. Analysing this filter, a Gauss windowed Sinc filter was obtained which presents a similar performance, but a better computation time. For the calibration of the accelerometer and the gyroscope, several approaches were executed using a pendulum, an inclinometer and an encoder which measures the angular position (after improving its signal resolution). It is possible to relate the acceleration and the angular velocity with the angular position. The gyroscope will have an error in the order of 1.6%. Although the method used for the accelerometer calibration does not allow a very accurate prediction of the absolute error, it presents good results with mean deviations in the order of 0.0044 g. The result of the project consists of a robust and innovative system that measures physical parameters with good accuracy and will integrate an ocean data acquisition system.

Keywords: ODAS, Readonly filesystem, Gaussian Sinc filter, IoT, Data analysis

1 Introduction

The presented article aims to develop a data acquisition and communications system for a wave energy conversion (WEC) moored buoy that will be launched on the Atlantic Ocean. The system will acquire both oceanographic and turbine/generator data. Its power supply will come from the wave energy conversion.

Acquiring data in the ocean is often very difficult and expensive. The environment can be very adverse, due to the waves, wind, currents and seawater corrosion. Ocean data acquisition systems (ODAS) are defined as an installation, platform, buoy or any other device with appropriate equipment to acquire data in the sea about the marine environment or the atmosphere [2]. Usually, ODAS exist on drifting or moored buoys, fixed platforms, ice drifters, island stations, coastal stations or profiling floats. From all the presented mechanisms, the moored buoy is considered as the most capable of acquiring real-time data of a fixed geographical region at an adequate rate. It can give good reference values for properties measured in satellites and has the advantage (over ships and drifting buoys) of remaining in the same geographical place. On the other hand, the CAPEX investment on moored buoys – which goes from the expenditures in the buoy's construction until the deployment and mooring – is very high. Costs can be reduced through the reutilisation of the buoy, more durable materials in its construction and better power supplies such as battery banks, solar or wind power and waves.

One major problem of moored buoys ODAS is the fact that they often have periods when they lack sufficient power supply. For example, the use of solar panels combined with an insufficient energy storage capability. This might cause the data acquisition and transmission to be intermittent. Because the wave energy availability on the ocean is high during day or night, a buoy that extracts energy from the waves will have an advantage over other ODAS.

In oceanography, data acquisition systems are especially important to collect data from the ocean for environmental and biological studies. Studying the sea has been important since pre-historic times. Until a few centuries ago, the purpose of oceanography was to understand the tides and currents for navigation and fishery. Today, understanding maritime ecosystems, forecasting the weather and understanding the geological, physical and chemical properties of the sea also integrate this science.

Data Acquisition is defined by a process in which a physical phenomenon is transformed into an electrical signal so that it can be converted into a digital format, analysed and stored by a computer [3]. This stored information can be useful for multiple

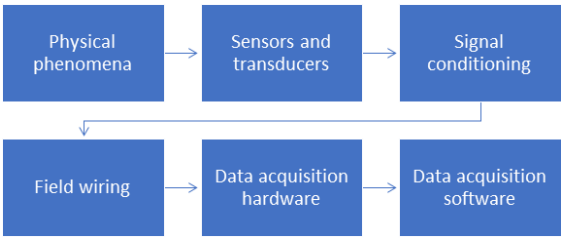

Figure 1: Data Acquisition System process.

purposes.

The model of the Fig. 1 is observed in most data acquisition systems, nowadays. The computer used for the data acquisition was a single-board Banana Pi M3. It reads measurements from the accelerometer, gyroscope and magnetometer sensor MPU-9150 and from an Analogue-to-digital converter (ADC) which converts the analogue signals from an integrated circuit temperature sensor LM35 DZ and a relative humidity sensor HIH 4000.

1.1 Data acquisition software

The data acquisition program consists on using a circular buffer with multithreading. The process of writing data to a hard disk takes time, and data reading from the sensors is fast. To not cause delays in data reading, we can store it in a buffer while data is being written from it to a file. Multithreading in programming is the ability to run several commands concurrently. While one process is reading data from the sensor to the buffer, another is writing data from the buffer to a file at the same time.

One way to manage the input and output of information of a buffer is using the FIFO circular method. FIFO stands for "first-in-first-out". It defines that the "oldest" data that was stored in the buffer must be the next to leave it. In a circular buffer, when the last input data is stored in the last free space of the buffer, the next free space of the buffer will be its first. If an input has to enter a space which is not free yet, it must wait. If an output has to leave the space to the file, but the space is empty, it must wait until data enters it. If the reading and writing processes access the same space at the same time it can cause data corruption which will lead to incorrect information stored. In other words, concurrent access to a space is not allowed.

To implement a shared circular buffer between two processes is not an easy task. Not only the buffer must be shared, but also, each process must know which space of the buffer the other one is using. In this case, a shared structure contains not only the buffer, but indicators such as the next available space for input, the next available space for output, the number of occupied spaces, an indicator if the buffer is empty, an indicator if the buffer is full and a condition lock variable that define if a process is allowed to read or write. Each process can alter not only the buffer but also the indicators.

A storage unit can be corrupted if, while data is being written to it, the power supply fails. To guarantee that the ODAS is always accessible, the storage was divided in two parts: the operative system is in a storage unit with the attribute "read-only filesystem", where data cannot be written to it; the sensors data are written to a a different storage unit with the "read-write filesystem" attribute. While the second unit can be corrupted, the first cannot, which means that the system will always be accessible.

2 Signal filtering

There two main categories of filters: the causal and the non-causal. The causal filters only use present and past data (in relation to the measured instant) and may be used in real-time. Non-causal filters use past, present and future information about the sensor's signal to filter the present point, and can only be used in post-processing. Data resulting from causal filters usually have a phase lag. This article describes solely non-casual filters.

2.1 Savitzky-Golay filters

The SG filters [1] try to locally fit the unfiltered signal in an n^{th}-degree polynomial. When modelling the signal using less points that the total, the polynomial cannot follow every point, but it will follow a tendency, resulting in a smoothed signal. The unfiltered signal f[i] can be approximated by a polynomial p[i], where:

$$p_i = \sum_{k=0}^{N} a_k i^k. \tag{1}$$

To find the polynomial coefficients a_k, the following operation is used:

$$\begin{bmatrix} {i_0}^k & \dots & i_0 & 1 \\ {i_1}^k & \dots & i_1 & 1 \\ \dots & \dots & \dots & \dots \\ {i_n}^k & \dots & i_n & 1 \end{bmatrix} \begin{bmatrix} a_k \\ a_{k-1} \\ \dots \\ a_0 \end{bmatrix} = \begin{bmatrix} f_1 \\ f_2 \\ \dots \\ f_n \end{bmatrix}. \tag{2}$$

The matrix of the Eq. (2) on the left-hand side is called Vandermond matrix. In other notation, this equation can be represented by:

$$A\,y = f. \tag{3}$$

To solve this equation simply multiply both sides by A^T on the left.

$$A^T\,A\,y = A^T\,f. \tag{4}$$

The polynomial coefficients in vector y:

$$y = \left(A^T\,A\right)^{-1}\,A^T\,f. \tag{5}$$

The filter depends only on the degree of the polynomial and the size of the window. The higher the degree of the polynomial, the higher will the steepness of the roll-off be and the attenuation will be better. The polynomial interpolation, in some cases, can be a problem. When the degree of the approximation polynomials is very high, the resulting Vandermonde matrix is known to become very ill-conditioned. In the case of least squares problems, it becomes even more difficult to compute accurately the polynomial coefficients. To show this, let us remember the definition of conditioning number of a matrix.

$$\text{cond}\,(A) = \|A\|\|A^{-1}\|. \tag{6}$$

The conditioning number of the matrix of Eq. (4) is

$$\begin{aligned}\text{cond}\left(A^T A\right) &= \|A^T A\|\left\|\left(A^T A\right)^{-1}\right\| \\ &= \|A^T A\|\|A^{-1}A^{-T}\| \\ &\sim \|A^T\|\|A\|\|A^{-1}\|\|A^{-T}\| \\ &\sim \|A\|^2\|A^{-1}\|^2 = \text{cond}(A)^2\end{aligned} \tag{7}$$

2.2 Legendre-based filters

To overcome the instability problems of computing least squares problems with high-order polynomials, a different solution based on Legendre polynomials is purposed. The idea is to use the orthogonality property of the polynomials to simplify the computations. As such, let us approximate of a function $f(\tau)$ with a set of $n+1$ Legendre polynomials, P_i,

$$f(\tau) = \sum_{i=0}^{n} a_i P_i(\tau). \tag{8}$$

such that $\tau \in [-1, 1]$. To compute the parameters a_i of the polynomial approximation using least-squares, one must to minimize the error function.

$$E(a_0, \ldots, a_n) = \int_{-1}^{1} \left(\sum_{i=0}^{n} a_i P_i(\tau) - f(\tau) \right)^2 \mathsf{d}\tau. \tag{9}$$

The minimum with respect to a_k occurs at

$$\frac{\partial}{\partial a_k} E(a_0, \ldots, a_n) = 0, \tag{10}$$

giving

$$2\int_{-1}^{1} P_k(\tau) \left(\sum_{i=0}^{n} a_i P_i(\tau) - f(\tau) \right) \mathsf{d}\tau = 0. \tag{11}$$

Rearranging, yields

$$\int_{-1}^{1} P_k(\tau) \left(\sum_{i=0}^{n} a_i P_i(\tau) \right) \mathsf{d}\tau = \int_{-1}^{1} P_k(\tau) f(\tau) \mathsf{d}\tau. \tag{12}$$

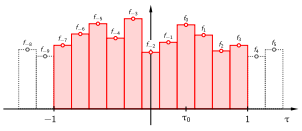

Figure 2: Piecewise function, f_l, with $N_T = 11$, $N_L = 7$ and $N_R = 3$.

Due to the orthogonality of the Legendre polynomials, Eq. (12) simplifies to

$$a_k \int_{-1}^{1} P_k(\tau)^2 \, \mathsf{d}\tau = \int_{-1}^{1} P_k(\tau)\, f(\tau) \mathsf{d}\tau. \tag{13}$$

The value of the integral on the left-hand side is given by

$$\int_{-1}^{1} P_k(\tau)^2 \, \mathsf{d}\tau = \frac{2}{2k+1}. \tag{14}$$

As a result, the value of the coefficient a_k is

$$a_k = \frac{2k+1}{2} \int_{-1}^{1} P_k(\tau)\, f(\tau)\, \mathsf{d}\tau. \tag{15}$$

For the sake of simplicity, let us assume a uniform discretization of the time interval $\tau \in [-1, 1]$ in N_T time intervals I_l, $l \in \{-N_L, \ldots, N_R\}$, such that

$$N_T = N_L + N_R + 1. \tag{16}$$

Defining the centre of the time interval I_l by τ_l,

$$I_l = \left[\tau_l^-, \tau_l^+\right], \tag{17}$$

where

$$\tau_l^{\pm} = \tau_l \pm \Delta, \tag{18}$$

and

$$\Delta = \frac{1}{N_T}. \tag{19}$$

The Legendre polynomials are continuous functions but the digital data represents $f(\tau)$ only at discrete points. As a first approximation, a piecewise constant representation of the function $f(\tau)$ in each time interval I_l is used, such that

$$a_k = \frac{2k+1}{2} \sum_{l=-N_L}^{N_R} f_l \int_{I_l} P_k(\tau)\, \mathsf{d}\tau. \tag{20}$$

The value $\hat{f}$ of the filtered function at the centre

$$\tau_0 = \frac{N_L - N_R}{N_T}, \tag{21}$$

of the time interval I_0 is computed using

$$\begin{aligned}\hat{f}_0 &= \sum_{i=0}^{n} a_i\, P_i(\tau_0) \\ &= \sum_{i=0}^{n} \frac{2i+1}{2} \left(\sum_{l=-N_L}^{N_R} f_l \int_{I_l} P_i(\tau)\, \mathsf{d}\tau \right) P_i(\tau_0).\end{aligned} \tag{22}$$

The idea is illustrated in Fig. 2 where $N_T = 11$ and $N_L = 7$ and $N_R = 3$. Writing Eq. (22) as a weighted sum of the function values, f_l, gives

$$\hat{f}_0 = \sum_{l=-N_L}^{N_R} b_l \, f_l, \tag{23}$$

where the coefficients of the filter are determined by

$$b_l = \sum_{i=0}^{n} \frac{2i+1}{2} P_i(\tau_0) \int_{I_l} P_i(\tau) \, \mathsf{d}\tau. \tag{24}$$

Evaluating analytically the integrals of (24) :

$$\begin{aligned} b_l = \Delta + \frac{1}{2} \sum_{i=1}^{n} P_i(\tau_0) \left(P_{i+1}(\tau_l^+) \; - P_{i+1}(\tau_l^-) \right. \\ \left. - P_{i-1}(\tau_l^+) \; + P_{i-1}(\tau_l^-) \; \right). \end{aligned} \tag{25}$$

Similarly, the value of m-th derivative $\mathsf{d}^m \hat{f}/\mathsf{d}\tau^m$ of the filtered function at the centre of the time interval I_0 is computed using

$$\begin{aligned} \frac{\mathsf{d}^m \hat{f}_0}{\mathsf{d}\tau^m} &= \sum_{i=0}^{n} a_i \frac{\mathsf{d}^m P_i}{\mathsf{d}\tau^m}(\tau_0) \\ &= \sum_{i=0}^{n} \frac{2i+1}{2} \left(\sum_{l=-N_L}^{N_R} f_l \int_{I_l} P_i(\tau) \, \mathsf{d}\tau \right) \frac{\mathsf{d}^m P_i}{\mathsf{d}\tau^m}(\tau_0), \end{aligned} \tag{26}$$

which yields

$$\frac{\mathsf{d}^m \hat{f}_0}{\mathsf{d}\tau^m} = \sum_{l=-N_L}^{N_R} c_l^{(m)} \, f_l, \tag{27}$$

where the coefficients of the filter are given by, for $m > 0$,

$$\begin{aligned} c_l^{(m)} = \frac{1}{2} \sum_{i=1}^{n} \frac{\mathsf{d}^m P_i}{\mathsf{d}\tau^m}(\tau_0) \left(P_{i+1}(\tau_l^+) - P_{i+1}(\tau_l^-) \right. \\ \left. - P_{i-1}(\tau_l^+) + P_{i-1}(\tau_l^-) \right). \end{aligned} \tag{28}$$

The Legendre polynomials are known to satisfy the following relation, for $i > 0$,

$$(2i+1) P_i(\tau) = \frac{\mathsf{d}}{\mathsf{d}\tau} \left(P_{i+1}(\tau) - P_{i-1}(\tau) \right). \tag{29}$$

Integrating (29) in I_l :

$$\begin{aligned} \int_{I_l} P_i(\tau) \, \mathsf{d}\tau &= \frac{1}{2i+1} \int_{\tau_l^-}^{\tau_l^+} \frac{\mathsf{d}}{\mathsf{d}\tau} \left(P_{i+1}(\tau) - P_{i-1}(\tau) \right) \mathsf{d}\tau \\ &= \frac{1}{2i+1} \left(P_{i+1}\left(\tau_l^+\right) - P_{i+1}\left(\tau_l^-\right) - \right. \\ &\left. P_{i-1}\left(\tau_l^+\right) + P_{i-1}\left(\tau_l^-\right) \right). \end{aligned} \tag{30}$$

For $i = 0$,

$$\int_{\tau_l^-}^{\tau_l^+} P_0(\tau) \, \mathsf{d}\tau = 2\Delta, \tag{31}$$

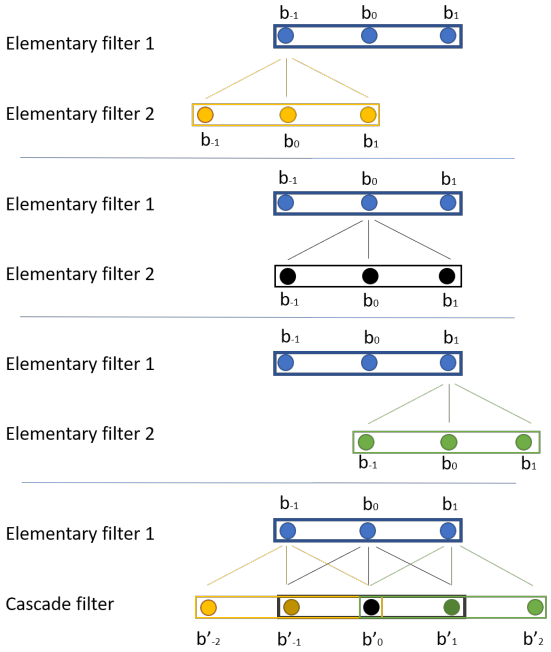

Figure 3: Obtaining a two layer cascade filter coefficients.

since $P_0(\tau) = 1$.

Finally, the integrals that appear in Eq. (24) can be evaluated analytically using

$$\begin{aligned} \sum_{i=0}^{n} \int_{I_l} P_i(\tau) \, \mathsf{d}\tau = 2\Delta + \sum_{i=1}^{n} \frac{1}{2i+1} \left(P_{i+1}(\tau_l^+) - \right. \\ P_{i+1}(\tau_l^-) - P_{i-1}(\tau_l^+) + \\ \left. P_{i-1}(\tau_l^-) \right). \end{aligned} \tag{32}$$

3 Cascade filtering

The recursive or cascade filtering is a sequential combination of multiple elementary filters. The cascade filter response on the frequency domain is the multiplication of the responses of all elementary filters. The process to obtain the cascade filter coefficients is explained by Fig. 3. It uses an example of a cascade filter formed by the convolution of two equal elementary filters of three points. The cascade coefficients are represented below

$$b'_{-2} = b_{-1}, \tag{33}$$
$$b'_{-1} = b_{-1} \, b_0 + b_0 \, b_{-1}, \tag{34}$$
$$b'_0 = b_{-1} \, b_1 + b_0 \, b_0 + b_1 \, b_{-1}, \tag{35}$$
$$b'_1 = b_0 \, b_1 + b_1 \, b_0, \tag{36}$$
$$b'_2 = b_1. \tag{37}$$

Figs. 4 and 5 present the frequency response and filter coefficients for several LB filters and the resulting cascade filter. All are made from Legendre

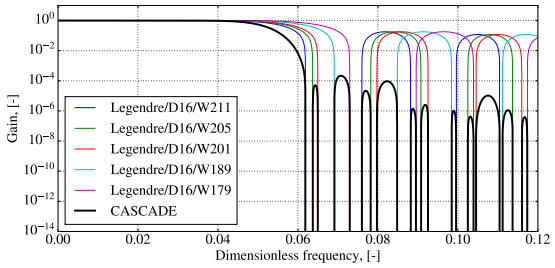

Figure 4: Cascade filter obtained using Legendre filter of degree 16 with windows of 211, 205, 201, 189 and 179 points.

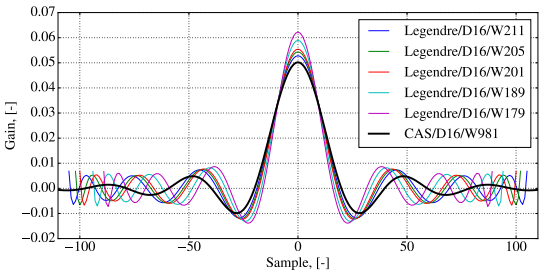

Figure 5: Legendre-based filters in time domain.

polynomials with a 16^{th} degree order, D. The window size, W, varies from 179 to 211 for the LB filters and it is 981 for the cascade filter. The cascade filter ripple is much lower than the elementary LB filters. This will translate into very low gains in the stop-band for the cascade filter. On the pass-band, the gains of the cascade filter will start to decay at the same frequency of the elementary filter that decays first. Multiplying the gains in the stop-band, a cascade filter is obtained with the side-lobes a lot more attenuated in comparison with elementary filters. This is the result of choosing single filters with windows of 205, 201, 189 and 179 points which have cut-off frequencies within the first lobe of the filter with a window of 211 points. Figs. 4 and 5 also show that if several low-pass elementary filters with different cut-off frequencies are combined in a cascade filter with better properties than the elementary filters is obtained. Summarizing, the cascade filter has a better attenuation and roll-off than the elementary filters.

3.1 Gaussian Sinc filter

One of the things that was noticed in the Fig. 5 was the fact that the shape of the cascade function is very similar to a sinc function

$$\mathsf{sinc}(x) = \frac{\sin(\pi\, x)}{\pi\, x} \tag{38}$$

Another curious observation is the fact that the decay of the oscillations of the cascade filter towards away from the centre had a behaviour similar to an exponential function.

The sinc filter is an ideal filter and it is the inverse Fourier transform of a Heaviside step function in the frequency domain [5]. It can make the drop exactly at the cut-off frequency (the transition-band is zero). Its gain is unitary in the pass-band and null in the stop-band.

The sinc function, Eq. (38), never reaches an amplitude equal to zero when $i \to \pm\infty$. Since the computers can not process an infinite series, to transform the sinc function into a windowed function one must truncate it, resulting in

$$h[i] = \frac{\sin(\alpha\, i)}{i}, \qquad i \in \{-M, \ldots, 0, \ldots, M\}. \tag{39}$$

Outside the central interval, the gain is zero. This creates a new problem: it is very difficult to model a piecewise discontinuous function (such as the filter response in the frequency domain) by a finite sine wave in time, due to Gibbs oscillations. The response instead of being an ideal filter will show overshoots and undershoots in the pass-band.

To solve this problem one can multiply the truncated sinc function by a window function. A Gauss window will be used to produce a Gaussian Sinc filter. The result will not be an ideal filter. The transition bandwidth will not be zero, but the oscillations at the pass-band and stop-band will be largely smoothed without compromising the desired filter properties.

The parameters that control the sinc function are the cut-off frequency and the window size after truncation. The cut-off frequency is proportional to the coefficient α. One characteristic of the cut-off frequency is the fact that it is measured at the middle of the gain drop during the transition band, instead of the usual 3 dB. This happens because the sinc filter is symmetrical between the pass-band and the stop-band.

The number of points (or window size), 2M+1, are chosen knowing that the gain coefficients calculated must be centred (i.e., $i \in \{-M, \ldots, 0, \ldots, M\}$). The number of points control the transition band size. The higher is M, the shorter will be the transition band. A good approximation of the transition bandwidth (BW) can be seen in the Eq. (40) [4]

$$BW = \frac{4}{M}. \tag{40}$$

To attenuate the truncation problems, the sinc filter convolves with a Gauss window.

$$g[i] = \frac{1}{\sqrt{2\,\pi\,\sigma}}\, e^{-\frac{i^2}{2\,\sigma^2}}. \tag{41}$$

The Gauss window has the ability to prevent overshoot and undershoot. This means that there are no oscillations in pass-band and the stop-band is very smooth. On the other hand, a Gauss window slows the roll-off of the Sinc filter. To obtain the Gaussian sinc filter, a convolution between the Gauss and the

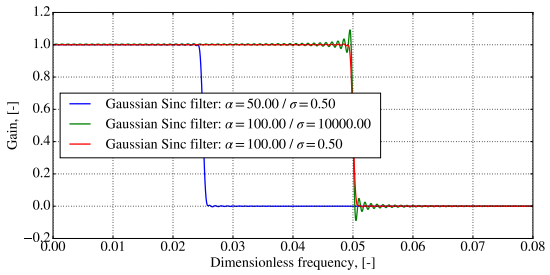

Figure 6: Gaussian Sinc filter response in frequency.

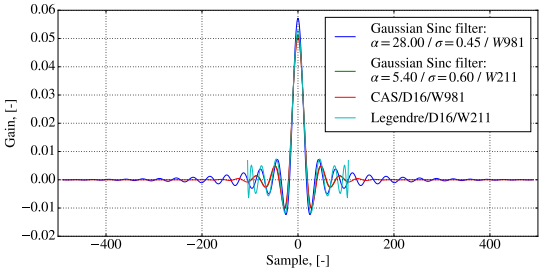

Figure 7: Legendre-based, Gauss Sinc and cascade filters in time domain.

truncated sinc filters is performed. The coefficient K, in the Eq. (42), normalizes the result.

$$hg[i] = K\, h[i] * g[i]. \tag{42}$$

The Gauss window will attenuate the oscillations of the sinc filter in both pass-band and stop-band. The sinc function will allow a narrow transition band.

The Fig. 6 presents three different Gaussian Sinc filters in the frequency domain. The red curve represents the reference design parameters. In comparison to the red curve, the blue curve has a lower coefficient α. Since the cut-off frequency is proportional to α, if α decreases, the cut-off frequency will also decrease. Because the standard deviation is not changed, the Gaussian smoothing is the same. It is visible that the stop-band and pass-band are symmetrical. For that reason, the cut-off frequency is the frequency at which the gain of the Gaussian Sinc filter is 0.5.

The green curve has the same α coefficient as the red curve. Therefore, both curves have the same cut-off frequency. On the other hand, the standard deviation σ is much higher on the green filter than on the red one. In other words, the Gauss window contribution to the filter is lower. For that reason, the resulting filter will behave similarly to a truncated sinc filter. This behaviour consists on a narrower transition-band at the cost of the undershoot and overshoot in the pass-band and the stop-band.

3.2 Filter comparison

The Fig. 7 shows a comparison of studied filters in time domain. Two of them are Gaussian Sinc

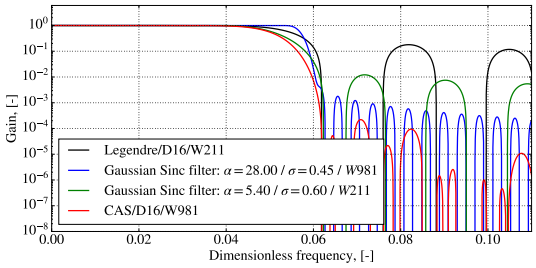

Figure 8: Legendre-based, Gauss Sinc and cascade filters in frequency domain.

filters, with different α coefficients, different standard deviations, σ and different window sizes, W. The cascade filter of 16^{th} degree, with a window with 981 points and the LB filter of 16^{th} degree, with a window with 211 points from Fig. 5 are also present. One of the Gauss Sinc filters have the same window size as the cascade filter. The other Gaussian Sinc filter as the same window size as the LB filter. The filter that shows more instability is the LB filter. This will cause a poor attenuation in the stop-band, compared to the other filters. On the opposite side, the cascade filter presents a very good attenuation. This is proven in Fig. 8.

In Fig. 8, comparing the Gauss Sinc filters, both of them have a standard deviation, σ, of the same order. They differ mostly on the α coefficient, which results in a lower cut-off frequency the filter with lower α. The Gaussian Sinc function with a larger window will have a much narrower transition-band. Comparing the cascade filter with the LB, the cascade provides a much better attenuation. The LB filter has a steeper roll-off than the smaller window Gaussian Sinc filter. Despite this advantage, the lobes of the stop-band of the LB filter reach a gain in the order of 10% which is very high. On the other hand, the smaller window Gaussian Sinc filter lobes can reach a gain of the order of 0.1%. The cascade and the larger window Gaussian Sinc filters are the ones with the better attenuation in the stop-band. Both have the same window size. The cascade filter oscillates closer to zero. On the other hand, the stop-band in both filters is so low that, in practice, there is no difference between the two in terms of attenuation. On the other side, the Gaussian Sinc filter has the steepest roll-off and its computation is faster.

The definition of best filter differs from case to case. Both the cascade and the Gaussian Sinc filter would fit the purpose of this project. Since both have a very good attenuation performance, the criterion used to select a filter was the roll-off performance and computation speed. In these fields, the Gaussian Sinc proved to be the best and, therefore, will be the one used.

4 Calibration

The calibration of the accelerometer and gyroscope required a pendulum and a mechanism to measure its angular position (encoder and inclinometer). The pendulum has a total height of 1.98 metres. The encoder used was the AEDB-9140.

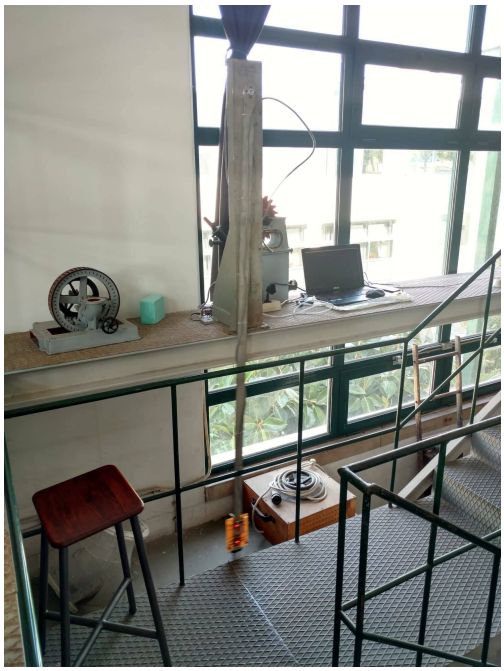

Figure 9: Pendulum.

4.1 Gyroscope

The gyroscope is calibrated using the angular velocity calculated with the encoder. The procedure consists on dropping the pendulum from a certain height and measuring the encoder counts while the gyroscope measures the angular velocity in the same direction as the pendulum rotation. The test only finishes when the pendulum stops. Both measures must be taken at the same time. The sampling frequency used was 400 Hz. From the encoder, the angular velocity is calculated in radians per second. From the gyroscope, the angular velocity is measured in LSB. Calculating a parabolic regression between the both signals, to avoid a small phase error, only the peak values of each were used. From there, two sets of calibration coefficients are obtained (one for the upper peaks and another for the lower peaks). The final coefficients are the average of each pair of coefficients from the regression. As it is seen in Figs. 10(a), 10(b) and 10(c), the second order coefficients of each regression have different signs, which means that the average must be calculated for the absolute values. Although the datasheet present a linear relation between the angular velocity in LSB and in degrees per second of 1.33×10^{-4} rad/s/LSB, the fit made here was quadratic. The linear coefficient of the quadratic fit

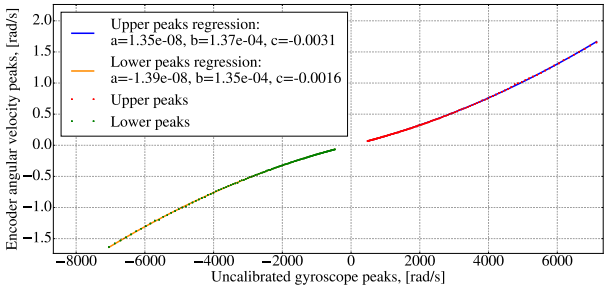

(a) X

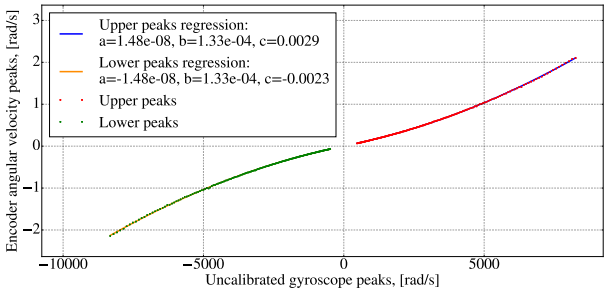

(b) Y

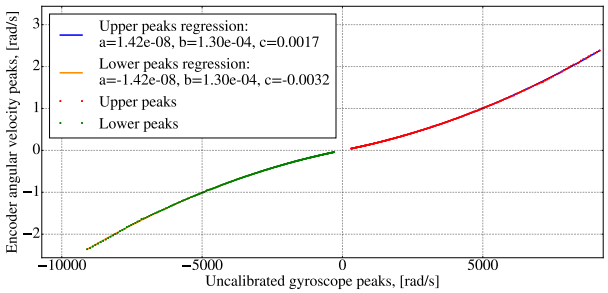

(c) Z

Figure 10: Angular velocity parabolic regression.

is very close to the datasheet coefficient. If the regression was only linear, the errors would be higher. The parabolic fit proved to be more successful. The last term of the calibration in Eqs. (43), (44) and (45) has the objective of removing the offset. The offset was calculated by making an exponential fit for the upper peaks and another for the lower peaks. The two fits must be equidistant to zero.

$$\dot{\theta}_x = \mathsf{sign}(\widetilde{\dot{\theta}}_x)\, 1.3727 \times 10^{-8}\, \widetilde{\dot{\theta}}_x^2 + 1.3586 \times 10^{-4}\, \widetilde{\dot{\theta}}_x - 7.6873 \times 10^{-4} - 0.0119 \quad (43)$$

$$\dot{\theta}_y = \mathsf{sign}(\widetilde{\dot{\theta}}_y)\, 1.4779 \times 10^{-8}\, \widetilde{\dot{\theta}}_y^2 + 1.3274 \times 10^{-4}\, \widetilde{\dot{\theta}}_y - 2.7953 \times 10^{-4} + 0.0282 \quad (44)$$

$$\dot{\theta}_z = \mathsf{sign}(\widetilde{\dot{\theta}}_z)\, 1.4226 \times 10^{-8}\, \widetilde{\dot{\theta}}_z^2 + 1.2974 \times 10^{-4}\, \widetilde{\dot{\theta}}_z - 7.2401 \times 10^{-4} - 6.1785 \times 10^{-5} \quad (45)$$

4.2 Accelerometer

To calibrate the accelerometer an inclinometer was used to measure the inclination angle of the pendulum in static positions. If the pendulum is static, the only force applied to the accelerometer is gravity. The radial and tangential accelerations can be calculated using only trigonometric relations from Eqs. (46) and (47) (where θ is measured by the inclinometer). Making a linear regression between the calculated acceleration and the accelerometer measurements, the accelerometer sensitivity is calculated.

The accelerometer is calibrated using the Eqs. (46) and (47).

$$\ddot{x}_{rad} = g\,\cos\theta \tag{46}$$

$$\ddot{x}_{tan} = g\,\sin\theta \tag{47}$$

Making the linear regression, the results in Eqs. (48), (49) and (50) are obtained.

$$\ddot{x} = 5.9778 \times 10^{-5}\,\widetilde{\ddot{x}} - 0.0224 \tag{48}$$

$$\ddot{y} = 6.0408 \times 10^{-5}\,\widetilde{\ddot{y}} - 0.0119 \tag{49}$$

$$\ddot{z} = 5.9832 \times 10^{-5}\,\widetilde{\ddot{z}} - 0.0426 \tag{50}$$

The linear regression itself already produces a coefficient of the zero order term that removes the accelerometer offset. The sensitivity from the datasheet is 6.1035×10^{-5}. It is very similar to the sensitivities calculated (linear term of the calibration).

As it is presented in Figs. 11(a), 11(b) and 11(c), the fitting errors and standard deviations σ are relatively low. This calibration has the disadvantage of using a small number of points for the fit. For that reason, it is difficult to certainly know if the calculated errors are actually true.

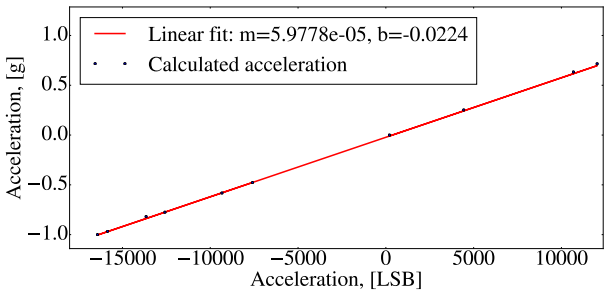

(a) X

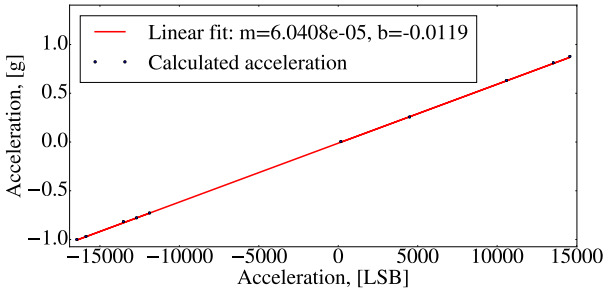

(b) Y

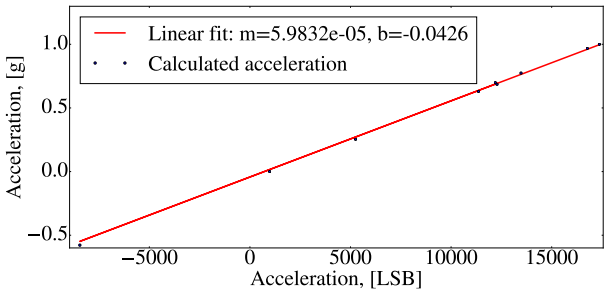

(c) Z

Figure 11: Acceleration linear regression.

5 Results

This section presents the results and discussion of the filter, calibration and the performance of the DAQ system.

5.1 Filter Implementation

The parameter for the chosen filter were: α coefficient equal to 5.6, the standard deviation σ is 0.5 and the window has 401 points. A cut-off frequency (proportional to α) too high can remove important information while if it is too low, the noise might not be well attenuated. A large window allows a better roll-off performance. It is important to maintain the standard deviation in a low value, since if it is high, it can cause the filter to behave simply as a truncated sinc filter.

The convolution blended the filter and the unfiltered gyroscope signal producing the filtered signal (Fig. 12).

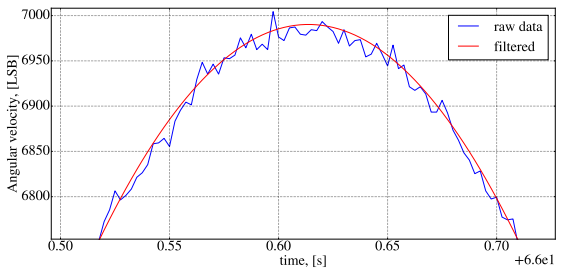

Figure 12: Filtered and unfiltered signals comparison.

Having seen the response in time, the signal in frequency domain can be represented. The frequencies that define the pendulum motion should have a

high amplitude. On the other hand, the frequencies at which the noise happens should have a lower amplitude. Fig. 13 shows that for frequencies between approximately 0.3 Hz to 0.6 Hz, the amplitudes are very high. This band defines the pendulum motion. The other frequencies present very low amplitudes. This means that the noise amplitudes are very low. The signal to noise ratio (SNR) in the Fig. 13 is very high.

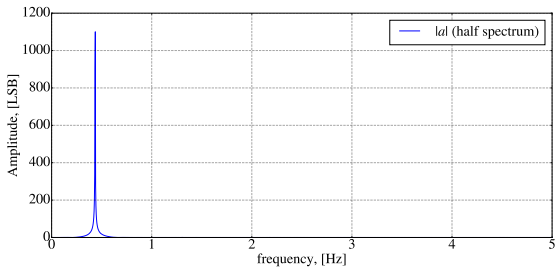

Figure 13: Filtered signal in the frequency domain.

5.2 Gyroscope

The method to obtain the results consisted on raising the pendulum to an amplitude of roughly 30^o and dropping it. With the encoder, the angular position is obtained and the angular velocity is calculated. The gyroscope will measure the angular velocity calibrated by Eqs. (43), (44), (45). The results are presented in Figs. 14(a), 14(b) and 14(c). Small errors and standard deviations σ were calculated. The error of the gyroscope calibration was 1.43% for the x axis, 1.62% for the y axis and 1.7% for the z axis. The standard deviation of the gyroscope calibration was 0.0063 rad/s for the x axis, 0.0090 rad/s for the y axis and 0.0066 rad/s for the z axis.

5.3 Accelerometer

The Figs. 11(a), 11(b) and 11(c) were obtain by aligning each axis with the vertical direction. The value of acceleration in this case must be 1 g (or -1 g if the axis is pointing downwards). For that reason, the acceleration calibrated it with the Eqs. (48), (49) and (50) can be measured. This calibration has the disadvantage of using a small number of points for the fit. However, it produces values very close from the expected. The measurements in the x vertical axis showed an error of 0.42 %. For the y vertical axis, the error is 0.60 %. For the z vertical axis, the error is 0.30 %.

6 Conclusions

This project achieved an innovative product for data acquisition systems. It uses low-cost components, which gives it some competitiveness advantage in relation to other types of ODAS in the market. Its objective is to be a system that can acquire data in any remote place. Because it uses small components (MEMS sensors), it can fit easily in any place, and its transportation and installation are simple. The system was designed to be very flexible and allow the integration of more analogue sensors.

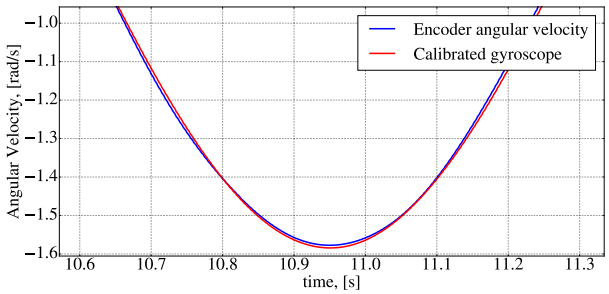

(a) X

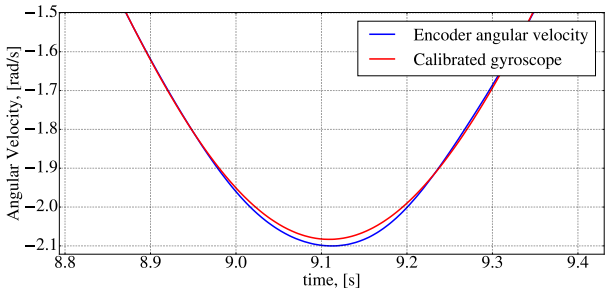

(b) -Y

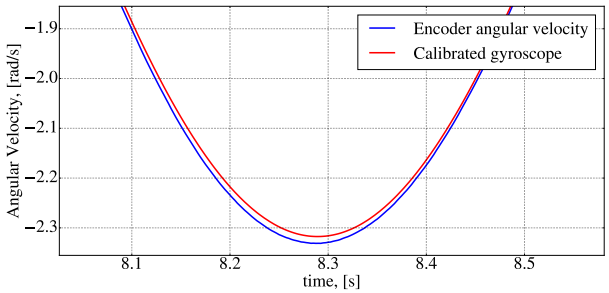

(c) Z

Figure 14: Calibrated gyroscope and encoder angular velocity comparison.

Filtering the signal was a very important step of this project. The filter selection process started with a study of the Savitzky-Golay filters. Its coefficients calculations were unstable. For that reason, Legendre-based filters were also addressed. A better performance could be obtained making a cascade filter out of elementary Legendre-based filters. The result was very good. Because the shape of the recursive filter was very similar to a sinc function, a sinc filter implementation was tried. Due to the fact that a sinc filter must be windowed to be implemented, it was truncated and its response caused overshoots and undershoots in the passband which prevented it from performing as an ideal filter. To overcome this issue, a convolution with a

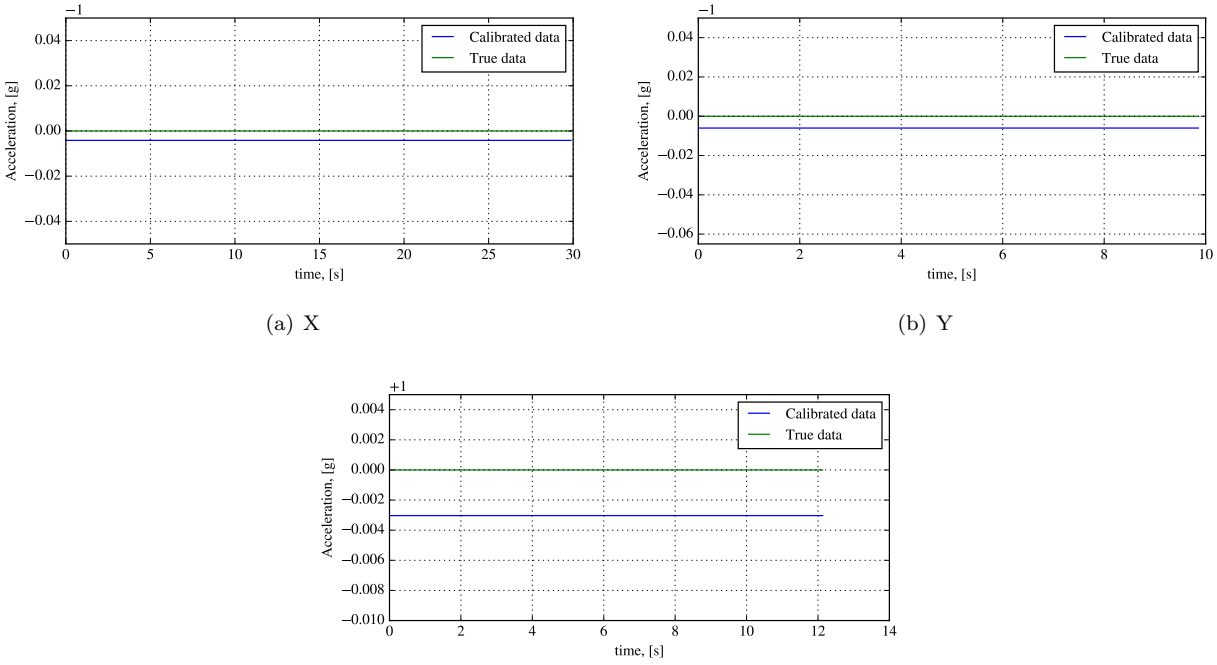

(a) X

(b) Y

(c) Z

Figure 15: Vertical axis acceleration measurement.

Gauss window was made. The result was very similar to the Legendre-based cascade filter. The transition band was narrower, and the attenuation difference between the two filters was negligible. And thus, the Gaussian Sinc filter was preferred since it is faster and more straightforward to implement.

The calibration of the gyroscope and accelerometer allowed an increase of the accuracy of the measurements. This makes the DAQ system more reliable.

In the future, a wider variety of sensors should be integrated into the system. The calibration of the accelerometer can be improved obtaining more calibration points with the pendulum in motion. In this case, not only the gravity acceleration is important, but also the friction, which is not trivial to model.

References

[1] J. Durão. Desenvolvimento de um Ondógrafo. Master's thesis, Instituto Superior Técnico, 2011.

[2] I. O. C. Group of Experts on the Legal Status of Ocean Data Acquisition Systems. Preliminary draft convention on ocean data acquisition systems (ODAS). In *Preparatory Conference of Governmental Experts to Formulate a Draft Convention on the Legal Status of ODAS*. UNESCO, 1972.

[3] S. Mackay, E. Wright, and J. Park. *Practical Data Communications for Instrumentation and Control*. Practical professional books from Elsevier. Elsevier Science, 2003.

[4] S. W. Smith. *The Scientist and Engineer's Guide to Digital Signal Processing*. California Technical Publishing, San Diego, CA, USA, 1997.

[5] M. Spiegel. *Schaum's Outline of Theory and Problems of Fourier Analysis, with Applications to Boudary Value Problems*. Schaum's outline series. McGraw-Hill, 1974.